Wind Energy

WIND ENERGY
Wind Energ. 2017; **20**:927–942
Published online 4 November 2016 in Wiley Online Library (wileyonlinelibrary.com). DOI: 10.1002/we.2071

RESEARCH ARTICLE

Estimation of the electric fields and dielectric breakdown in non-conductive wind turbine blades subjected to a lightning stepped leader

Yeqing Wang[1] and Olesya I. Zhupanska[2]

[1] Department of Mechanical and Industrial Engineering, The University of Iowa, Seamans Center for the Engineering Arts and Sciences, Iowa City, Iowa USA
[2] Department of Aerospace and Mechanical Engineering, University of Arizona, 1130 N. Mountain Ave., Tucson, Arizona USA

ABSTRACT

In this paper, the electric fields in the wind turbine blades due to the lightning stepped leader are studied, and the dielectric breakdown is assessed. The developed finite element analysis (FEA) includes the full length of the leader and enables one to incorporate various uniform and non-uniform charge density models. The lightning striking distance is calculated using the rolling sphere method. The electric field in a horizontal axis wind turbine with three blades representing Sandia 100 m All-glass Baseline Wind Turbine Blades (SNL 100-00) at three different lightning protection levels (LPL) is computed and compared to the dielectric breakdown strength of the blades. The dielectric breakdown strength of the blades is evaluated based on the experimental data. The results show that the tip region of the blade is the most vulnerable to the dielectric breakdown with the safety factor as low as 1.32 at LPL I. Copyright © 2016 John Wiley & Sons, Ltd.

KEYWORDS
lightning stepped leader; electric field; finite element analysis; wind turbine blade; dielectric breakdown

Correspondence
Olesya I. Zhupanska, Department of Aerospace and Mechanical Engineering, University of Arizona, 1130 N. Mountain Ave., Tucson, Arizona 85721, USA.
E-mail: oiz@email.arizona.edu
Contract/grant sponsor: National Science Foundation; contract/grant number: EPS-1101284.

Received 29 November 2015; Revised 7 September 2016; Accepted 9 October 2016

1. INTRODUCTION

Lightning strike poses a serious safety hazard for ground structures. The direct effects often include rapid temperature rise, melting or burning on the lightning attachment points, and mechanical damage due to the magnetic force and acoustic shock wave, etc.[1] In addition, dielectric breakdown is of concern in non-conductive structural components. Dielectric breakdown occurs when the strength of the electric field due to the lightning strike exceeds the dielectric breakdown strength of the structure. Dielectric breakdown is accompanied by both direct heat injection and Joule heating produced in the newly conductive structure that may lead to severe structural damage. Extensive use of the polymer matrix composite materials, which possess relatively low thermal conductivity, in the advanced light-weight structures makes these structures particularly vulnerable to the lightning strike. For instance, wind turbine blade damage accounts for the greatest number of losses, while lightning strikes are among the top two most frequently reported causes of loss in wind energy insurance claims in the United States.[2] Lightning protection of wind turbines has also been discussed in the literature.[3,4] The majority of the modern wind turbine blades are made of glass fiber polymer matrix composites[5] that are non-conductive. In addition, glass fiber polymer matrix composites possess relatively low thermal conductivity and are particularly vulnerable to the lightning strike. Therefore, careful analysis of the lightning-induced electric and thermal fields is critical for development of damage tolerant designs. The goal of this paper is to develop a computational procedure for calculation of the electric fields in wind turbine blades towards assessment of the probability of the dielectric breakdown.

A typical lightning consists of multiple return strokes, which are essentially electric current pulses. Prior to the first luminous return stroke, a leader, which is a conductive plasma channel, propagates from the cloud towards the ground. The function of the leader is to create a conducting path for the negative charge transfer from the cloud to a grounded structure. When the lightning leader tip arrives within a certain distance (lightning striking distance) of the grounded structure, the answering leader emitted from the grounded structure due to the electric field attempts to capture the approaching lightning leader. Once they are connected, the first lightning return stroke occurs. The leader prior to the first return stroke is called a stepped leader and is different from the subsequent strokes as it develops in virgin air. The first return-stroke current has a pulsed profile with a peak reaching up to hundreds kiloamperes. The electric current return-stroke wave heats and pressurizes the stroke channel leading to the rapid channel expansion, optical radiation and shock wave propagation in the outward direction. A short-duration pulsed current in a return stroke is typically followed by a continuous current, whose magnitude is about two orders of magnitude lower and three orders of magnitude longer than that of the initial pulsed current.

The overwhelming majority (90% and more) of cloud-to-ground lightning is the so-called downward negative lightning discharge, where negative charge is transported from the cloud to the ground.[6,7] As opposed to downward lightning discharge, the upward lightning discharge extends from the ground to cloud. As a structure height increases, the fraction of upward lightning discharges increases. Structures with heights ranging from 100 m to 500 m experience both upward and downward lightning discharges. It is reported[6] that upward lightning discharges constitute 50% in the 200 m tall structures and 80% in the 300 m tall structures. Therefore, both upward and downward lightning discharges are quite common in tall structures and are worth of consideration.

In the present study, a 250 m horizontal axis wind turbine with three blades representing Sandia 100 m All-glass Baseline Wind Turbine Blades (SNL 100-00) is considered and electric fields due to the lightning stepped leader of downward initiated lightning are studied.

There have been a number of studies on the lightning stepped leaders conducted in the past. Larigaldie *et al*.,[8] and Larigaldie[9] experimentally studied the propagation and electric current intensity of a typical lightning stepped leader. Larigaldie *et al*.[10] performed experimental and numerical investigation of the mechanisms of high-current pulses in lightning and long spark stepped leaders. Golde[11,12] developed a vertical lightning stepped leader model and was the first to introduce the non-uniform charge density of the leader into the analysis. Recently, Cooray *et al*.[13] derived a different non-uniform charge density distribution along the lightning stepped leader using the charge simulation method. The distribution has been validated using measurements of the in-field lightning incidents and was used to obtain a new expression for calculating the lightning striking distance (see equation (2) in Section 2.1 below), which was also found in better agreement with the physical measurements than the expression previously proposed by Uman[14] (see equation (1) in Section 2.1 below). All these leader models are for downward lightning flashes; the upward leader models have barely been reported.[15] The models developed by Uman[14] and Cooray *et al*.[13] are commonly used in the literature for the estimation of the electric fields due to the lightning stepped leaders. For instance, the Cooray *et al*.[13] model was used by Becerra[16] for calculation of the electric field distributions in complex ground structures. Lewke *et al*.[17] used the same model to determine the electric field in a wind turbine tower. Both studies[16,17] were performed using finite element analysis (FEA). One of the limitations of the aforementioned studies is that a computational domain in FEA were limited to the bottom part of the lightning stepped leader (close to the ground structure) and the upper part (close to the cloud) was not taking into account. Such choice of the computational domain leads to underestimation of the electric field, and therefore, to underprediction of the dielectric breakdown. The FEA conducted in the present study takes into account the full length of the lightning stepped leader (i.e. both the bottom and the upper parts), which enables accurate estimation of the electric field and occurrence of the dielectric breakdown.

The rest of the paper is organized as follows. In Section 2, an overview of the lightning stepped leader models is given. In Section 3, electric fields in the glass fiber reinforced polymer matrix wind turbine blades due to the lightning stepped leader are studied and compared to the dielectric breakdown.

2. OVERVIEW OF THE EXISTING LIGHTNING STEPPED LEADER MODELS

2.1. Lightning striking distance

Prior to the first lightning return stroke, a lightning stepped leader originates from the cloud and travels through the air towards the ground. When the lightning stepped leader approaches the ground, the ground structure emits answering leaders (streamers) due to the intensified electric field. The answering leader propagates to meet the lightning stepped leader and forms the first lightning return stroke.[6,18] The distance between the tip of the lightning stepped leader and the ground structure prior to the connection with the answering leader is called the lightning striking distance.

According to the IEC 61400-24 standard,[19] in the wind turbine blades longer than 20 m, the lightning striking distance can be defined using the rolling sphere method, where the radius of the rolling sphere attached to the ground structure is

considered to be equal to the lightning striking distance (see Figure 1). The radius is a function of the peak current of the lightning return stroke and is traditionally expressed as[14]

$$R = 10 \cdot I_{\text{peak}}^{0.65}, \tag{1}$$

where I_{peak} is the peak current of the lightning return stroke (in kA); R is the radius of the rolling sphere (in m).

More recently, Cooray *et al.*[13] suggested another expression for the radius of the rolling sphere, which agrees better with the recorded physical measurement data on the lightning striking distances:

$$R = 1.9 \cdot I_{\text{peak}}^{0.90}, \tag{2}$$

where R is the rolling sphere radius (in m) and I_{peak} is the peak current (in kA).

Table I shows the lightning striking distance calculated using equations (1) and (2) for three lightning protection levels (LPLs). The LPLs represent three different lightning severity levels as identified by the IEC 61400-24.[19] Peak current $I_{\text{peak}} = 200$ kA of the first short-duration stroke corresponds to LPL I, and $I_{\text{peak}} = 150$ kA and $I_{\text{peak}} = 100$ kA correspond to LPL II and LPL III, respectively. It can be seen in Table I that the striking distances calculated by equation (1) are around 1.5 times larger than those calculated by equation (2). Therefore, using equation (1) in a lightning stepped leader model will result in weaker electric field predictions at a ground structure compared to the predictions obtained when equation (2) is used. Because a more conservative estimate of the dielectric breakdown is obtained when a larger electric field is considered, equation (2) is used in this work to calculate the lightning striking distances.

It is worth mentioning that the lightning striking distance in conjunction with the rolling sphere method has been used in the previous studies of wind turbine blades.[17,18] As a side note, below we discuss the difference between the striking distance and the attractive radius, which is also widely used in the modeling of lightning attachment to the structures.

The attractive radius can be calculated as[20–22]:

$$R_a = 0.84 \cdot I_{\text{peak}}^{0.74} h_a^{0.6}, \tag{3}$$

where R_a is the attractive radius (in m), I_{peak} is the peak current (in kA) and h_a is the structure height (in m). There is a significant difference between lightning strike distance, R, as defined by equations (1) and (2), and lightning attractive radius, R_a, as defined by equation (3). The first depends on the charge of the downward conductor only, whereas the later takes into account also the size of the structure. Figure 2 shows the ratio R/R_a as a function of the structure height h_a for $I_{\text{peak}} = 100$ kA. Depending on the height of the structure, the striking distance magnitude can be larger or smaller than

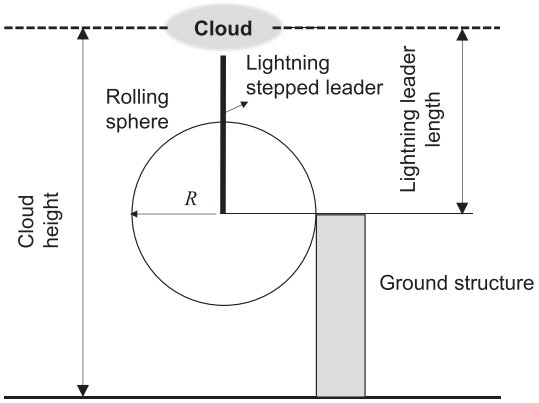

Figure 1. Lightning striking distance from stepped leader tip to a ground structure characterized using rolling sphere method.

Table I. Lightning striking distance for the lightning stepped leader.

LPL	Peak current, I_{peak} (kA)	Lightning striking distance (m)	
		From equation (1)	From equation (2)
I	200	313.09	223.71
II	150	259.69	172.68
III	100	199.53	119.88

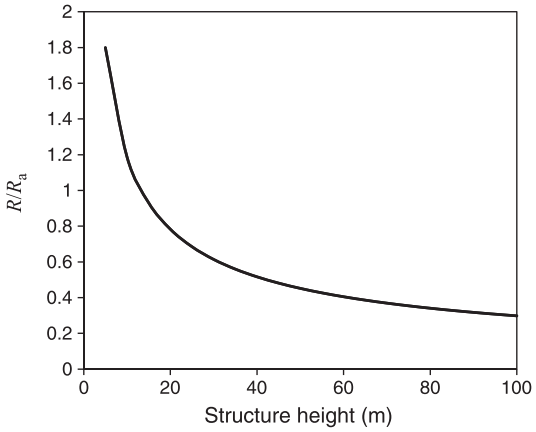

Figure 2. Ratio of striking distance to the attractive radius as a function of the structures height (I_{peak} = 100 kA).

the attractive radius magnitude. For tall structures (i.e. $h_a > 20$ m), the striking distance magnitude is smaller. Thus, using striking distance in a lightning stepped leader model will result in the prediction of a larger electric field at a ground structure, and, therefore, in a more conservative estimate for the dielectric breakdown.

2.2. Total charge associated with a lightning return stroke

According to Cooray *et al.*,[13] when a lightning stepped leader approaches the ground, the charge density of the leader depends on both the electric field due to the charge of the cloud and the electric field enhancement due to the presence of the ground. Figure 3 shows a simple lightning stepped leader model proposed by Cooray *et al.*[13] Here the cloud is represented by a conductive plane at potential V, and the ground is assumed to be a perfect conductor. Figure 3(a) shows a real leader approaching the ground with branched channels; Figure 3(b) shows an idealized vertical leader; Figure 3(c) shows negative charge, Q_l, along the leader before the return stroke; Figure 3(d) shows positive charge, Q_i, in the fully developed return stroke channel due to the field produced by the remaining negative charges in the cloud. The total positive charge, Q_t, entering from the ground to the fully developed return stroke channel during the first 100 μs is equal to the sum of the positive charge that neutralize the negative charge Q_l and the positive charge Q_i:

$$Q_{t,100\ \mu s} = |Q_l| + Q_i = 0.61 \cdot I_{peak}, \tag{4}$$

where $Q_{t,\ 100\ \mu s}$ is in C, and I_{peak} is the peak current, in kA.

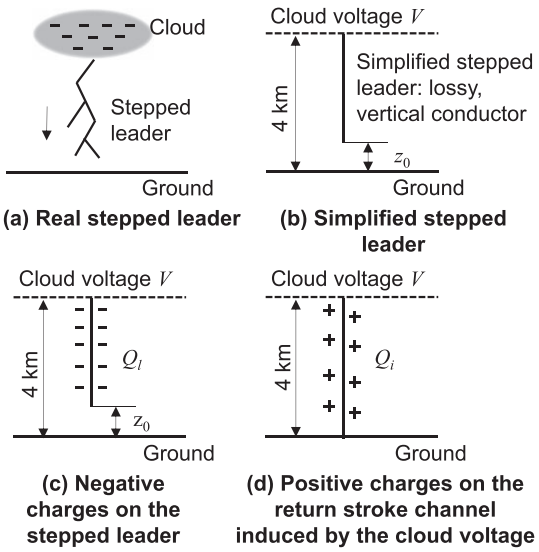

Figure 3. Simplified lightning stepped leader model proposed by Cooray *et al.*[13]

2.3. Charge density of a lightning stepped leader

Typically, a lightning stepped leader is idealized as a vertical line charge with a non-uniform charge density.[11–14,16,17] Golde[11,12] assumed that the charge density decreases exponentially along the lightning stepped leader from the tip to the origin of the leader in the cloud:

$$\lambda(\eta) = \lambda_0 e^{-\eta/\xi},\ 0 \le \eta \le L, \tag{5}$$

where $\lambda(\eta)$ is the charge density distribution (in C/m) along the leader and λ_0 is the charge density at the tip of the leader; η is measured in m; ξ is the decay height constant, $\xi = 1000$ m and L is the length of the leader (in m). In addition, $\eta = z - z_0$, where z is the vertical distance from the ground ($z = 0$ at the ground) and z_0 is the distance from the ground to the tip of the leader.

The total charge on the leader is obtained by integrating the charge density along the leader length. In the case of charge distribution (5), the total charge on the leader is

$$Q_l = \int_0^L \lambda(\eta) d\eta = \lambda_0 \xi \left[1 - e^{-L/\xi}\right], \tag{6}$$

where Q_l is the total charge (in C). The relationship between the peak current, I_{peak}, of the lightning return stroke and the charge density at the tip of the leader, λ_0, is[11,12]

$$\lambda_0 = 4.36 \cdot 10^{-5} I_{\text{peak}}, \tag{7}$$

where I_{peak} is measured in kA.

Cooray *et al.*[13] used the charge simulation method to derive a different non-uniform charge distribution along the lightning stepped leader:

$$\lambda(\eta) = a_0 \cdot \left(1 - \frac{\eta}{H - z_0}\right) \cdot G(z_0) \cdot I_{\text{peak}} + \frac{I_{\text{peak}} \cdot (a + b \cdot \eta)}{1 + c \cdot \eta + d \cdot \eta^2} \cdot F(z_0), \qquad 0 \le \eta \le L,\ z_0 \ge 10, \tag{8}$$

where η (in m) is the distance from the tip of the leader and $\eta = z - z_0$; $\lambda(\eta)$ is the charge density (in C/m); H is the height of the cloud (typically $H = 4000$ m); z_0 is the distance from the ground to the tip of the leader (in m); I_{peak} is the peak current of the return stroke (in kA); $G(z_0) = 1 - (z_0/H)$, $F(z_0) = 0.3\alpha + 0.7\beta$, $\alpha = e^{-(z_0 - 10)/75}$, $\beta = 1 - (z_0/H)$, $a_0 = 1.476 \cdot 10^{-5}$, $a = 4.857 \cdot 10^{-5}$, $b = 3.9097 \cdot 10^{-6}$, $c = 0.522$ and $d = 3.73 \cdot 10^{-3}$. It is also assumed that $z_0 > 10$ m. Cooray *et al.*[13] also found that charge distribution (8) was in a better agreement with physical measurements than charge distribution (5) proposed by Golde.[11,12] Figure 4 shows the charge density as a function of the height z for both cases at LPL III ($I_{\text{peak}} = 100$ kA). The distance from the tip of the leader to the ground is $z_0 = 250$ m and the length of the leader is $L = 3750$ m. As one can see, at the tip of the leader and at the vicinity of the cloud the charge densities calculated by equation (5) and (8) are similar. However, this is not the case for the bottom part of the leader away from the tip, where there is a significant discrepancy between two charge density distributions. Table II shows the total charge entering from the ground to the lightning channel, $Q_{t,\ 100\ \mu s}$, calculated using equation (4) and provided by IEC 61400-24 standard[19]

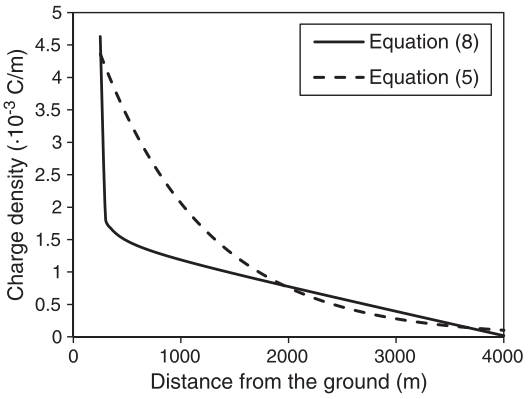

Figure 4. Charge density along the lightning stepped leader for the LPL III ($I_{\text{peak}} = 100$ kA, $z_0 = 250$ m).

Table II. Total charge entering from the ground to the lightning channel, $Q_{t,100\ \mu s}$ and total charge on the lightning stepped leader, Q_l.

LPL	$Q_{t,\ 100\ \mu s}$ (C)		Q_l (C)	
	IEC 61400-24[19]	From equation (4)	With non-uniform charge density (5)	With non-uniform charge density (8)
I	300	183	8.51493	5.70252
II	225	91.5	6.38619	4.27689
III	150	61	4.25746	2.85126

and the total charge on the leader, Q_l, in the case of charge density distributions (5) and (8). As one can see, the charge near the tip of the leader calculated as

$$Q_l^{tip} = \lim_{\eta \to 0} Q_l(\eta) = \lim_{\eta \to 0} \int_0^{\eta} \lambda(\eta) d\eta \tag{9}$$

is larger for distribution (8) due to the higher charge density near the tip (Figure 4). Because an electric field at a ground structure is mainly attributed to the charge at the bottom part of the lightning stepped leader, the electric field due to charge distribution (8) will be larger than the electric field due to charge distribution (5).

3. MODELING OF THE ELECTRIC FIELD IN A NON-CONDUCTIVE WIND TURBINE BLADE DUE TO A LIGHTNING STEPPED LEADER

In this section, FEA is developed to determine electric fields in a non-conductive wind turbine blade due to a lightning stepped leader. Electric fields are calculated for the blades representing Sandia 100 m All-glass Baseline Wind Turbine Blades (SNL 100-00).[23] Three different lightning protection levels, LPL I, LPL II and LPL III are analyzed. The FEA results are verified by comparisons with the analytical solution derived for the case of the leader with a uniform charge density. The electric fields obtained for the case of the leader with a non-uniform charge density (8) are compared to the dielectric breakdown strength of the blade to assess the conservativeness of the blade design. The dielectric breakdown strength is obtained using the experimental data reported in the literature.[18]

3.1. Problem formulation

We consider a horizontal axis wind turbine that is subjected to a lightning stepped leader (see Figure 5). Three blades, which are placed at a 150 m wind tower, represent Sandia 100 m All-glass Baseline Wind Turbine Blades (SNL 100-00).[23]

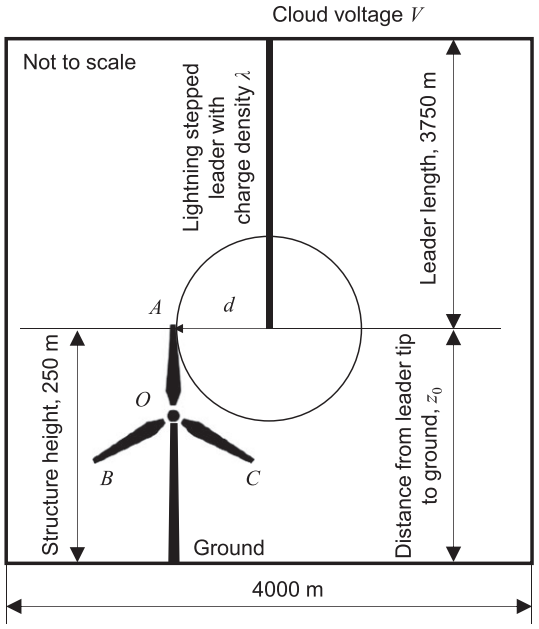

Figure 5. Interaction of a lightning stepped leader and a wind turbine: problem setup.

It is assumed that the leader is a vertical line charge that is perpendicular to the turbine axis and is located in the same plane with the blades (see Figure 5). Both uniform and non-uniform charge density distributions on the leader are considered. The length of each blade is 100 m, the overall structure height (the length of the blade together with the height of the tower) is 250 m, and the distance from the leader tip to the ground $z_0 = 250$ m. The length of the lightning stepped leader is 3750 m. The distance from the ground to the cloud is 4000 m. Cloud voltage is assumed to be constant. A typical 100 m wind turbine blade is equipped with multiple receptors, which are evenly distributed at the surface and are connected to the internal down conductor. The down conductor is installed inside the blade shell. Effects of the receptors and the down conductors are taken into account in the FEA study of Section 3.3, where ground potential is applied at the wind turbine exterior surface. Because blades are 100 m long, the rolling sphere method is used to obtain the lightning striking distance (denoted as d in Figure 5). It is assumed that the rolling sphere is tangentially attached to the tip of the blade OA. The lightning striking distance between the leader and blade OA is equal to the rolling sphere radius (2). Attachment to the tip is chosen because the tip region of the blade has the highest probability (>98%) to emit answering leaders.[18]

3.2. Electric field due to a lightning stepped leader with a uniform charge density: analytical solution

First, we consider a lightning stepped leader with the uniform charge density and find the electric field at the blade OA due to the leader (see Figure 6). If the ground is assumed to be at the infinity, the electric potential between a cloud and the ground is ignored, and the effects of the wind turbine receptors and down conductors on the electric fields are disregarded, the problem of finding the electric field along a wind turbine blade admits an analytical solution. The solution procedure is straightforward and similar to calculations of the electric field due to a charged lines and rods (see, e.g. Uman,[14] Tipler and Mosca[24]).

In accordance with the problem formulation described in Section 3.1, the leader is represented by a vertical line charge. The charge density is assumed to be uniform

$$\lambda = \frac{Q_l}{L}. \tag{10}$$

Here λ is the line charge density (in C/m); the total charge $Q_l(\eta)$ on the leader is calculated as $Q_l(\eta) = \int_0^L \lambda(\eta) d\eta$, where $\lambda(\eta)$ is non-uniform charge density (8), and L is the length of the leader (in m). The electric field due to the line charge is

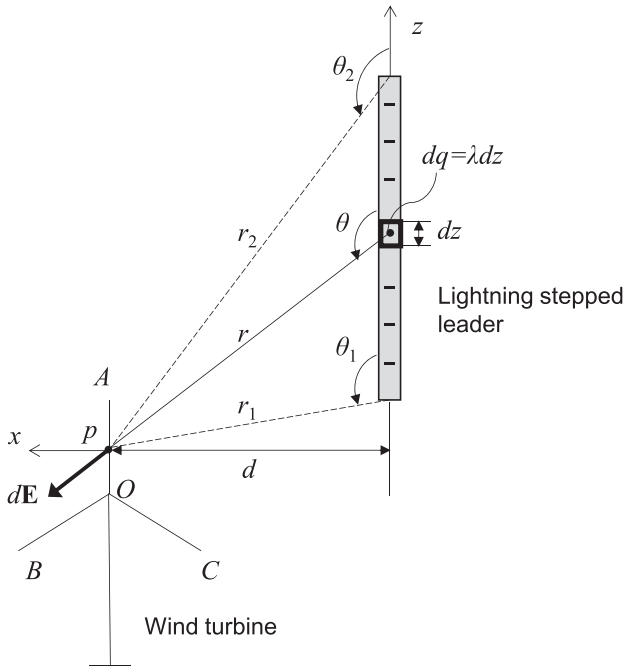

Figure 6. Electric field calculation at point p of the blade OA due to a uniformly charged lightning stepped leader.

calculated using Coulomb's law based on the assumption that the field due to an infinitesimal line charge element dq is the same as the field due to a point charge. Therefore, the electric field at an arbitrary point p of the blade OA due to the charge dq within dz is

$$dE = \frac{kdq}{r^2} = \frac{k\ \lambda dz}{r^2} = \frac{k\ \lambda d\ \theta}{d}, \tag{11}$$

where r is the distance from charge dq to the point p at the blade, $k = 9 \cdot 10^9\ \mathrm{N \cdot m^2 \cdot C^{-2}}$ is Coulomb's constant and $d = r \cdot \sin\theta$ is the lightning striking distance, which is equal to the rolling sphere radius (2). The x- and z-components of the electric field E from all the charge in the leader are

$$\begin{aligned} E_x &= \int_{\theta_1}^{\theta_2} \sin\theta \frac{k\ \lambda d\ \theta}{d} = -\frac{k\lambda}{d}(\cos\theta_2 - \cos\theta_1), \\ E_z &= \int_{\theta_1}^{\theta_2} \cos\theta \frac{k\ \lambda d\ \theta}{d} = \frac{k\lambda}{d}(\sin\theta_2 - \sin\theta_1). \end{aligned} \tag{12}$$

The magnitude (i.e. strength) of the electric field from all the charge in the leader is

$$|E| = \sqrt{E_x^2 + E_z^2} = \frac{2k\lambda}{d} \sin\frac{\theta_2 - \theta_1}{2}. \tag{13}$$

Here $|E|$ denotes the magnitude of the electric field (in V/m). Analytical solution (13) is essentially a distribution of the electric field due to a charged rod in an infinite space. The assumptions that were used to obtain this solution limit its applicability to the wind turbine blades. Nevertheless, this solution is useful as a checkpoint for the more realistic FEA-based models discussed in Section 3.3.

3.3. Finite element analysis of the electric fields due to a lightning stepped leader

In this section, FEA of the electric field in a wind turbine blade due to a lightning stepped leader is conducted. The problem formulated in Section 3.1 is solved using the COMSOL Multiphysics® FEA software. The FEA enables us to account for the effects of the non-uniform charge density distribution and finite ground that were not included in the analytical model considered in Section 3.2.

3.3.1. Implementation in COMSOL Multiphysics®.

The computational domain is a 3D parallelepiped containing a cutout in the shape of a wind turbine as shown in Figure 7. The dimensions of the cutout are determined by the dimensions of the wind turbine. Wind turbine blades and tower are assumed to be beams of square cross section, 2.5 m by 2.5 m. The computational domain represents the air between a cloud and the ground. The length and width of the parallelepiped are 4000 m. The depth is $L + z_0$, where $L = 3750$ m is the length

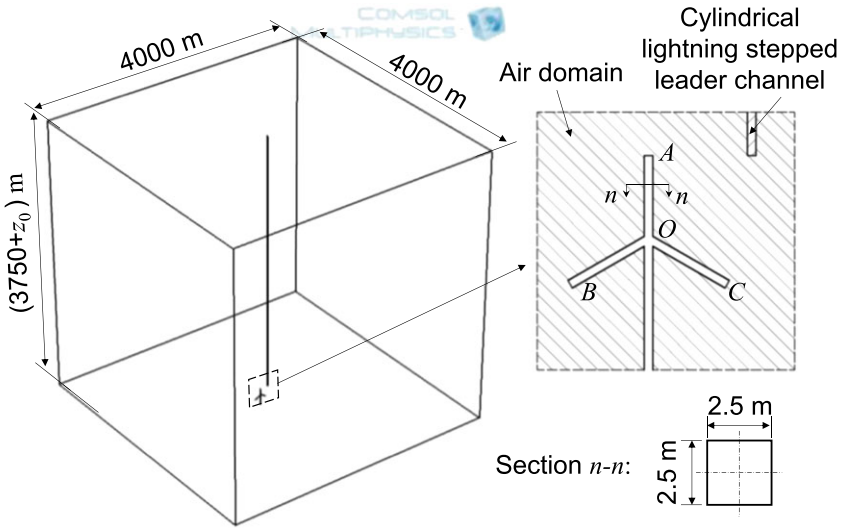

Figure 7. Problem setup in COMSOL. [Colour figure can be viewed at wileyonlinelibrary.com]

of the lightning stepped leader, and $z_0 = 250$ m is the distance from the tip of the leader to the ground. The lightning stepped leader is assumed to be a vertical cylindrical channel of length $L = 3750$ m and of radius $R_l = 5$ m. The radius is chosen as in.[17] The cylindrical leader channel is centrally placed in the 3D parallelepiped. Volume charge density $\rho_v = \lambda/\pi R_l^2$ where λ is the line charge density, is applied to the leader channel. Both uniform (10) and non-uniform (8) charge density distributions on the leader channel are considered. The lightning striking distance, d, as shown in Figure 5, is calculated using the rolling sphere radius (2).

As for boundary conditions, cloud voltage, V, is applied to the top surface of the parallelepiped. Ground potential is applied to the bottom surface of the parallelepiped and at the part of the domain boundary corresponding to the surface of the cutout (i.e. exterior surface of the wind turbine). In such a way, we account for the effects of multiple receptors and down conductors in the wind turbine on the electric field outside of the wind turbine. Open boundary conditions are assumed at all four vertical sides of the parallelepiped.

The present study is focused on estimating the static electric fields along blades *OA*, *OB* and *OC* induced by the lightning stepped leader. The analysis is conducted only for the defined domain (i.e. a 3D parallelepiped containing a cutout in the shape of a wind turbine). The domain (including the leader) is considered as an 'air material' defined in the COMSOL Material Library. The domain is meshed with 815 112 free tetrahedral elements. The average duration of each simulation is 128 s on a 4-core laptop PC.

3.3.2. FEA results for the case of the uniform charge density.

The lightning stepped leader with a uniform charge density is considered first. FEA is conducted for five different cases, when the ground is set at (i) infinity ($z_0 = \infty$), (ii) 250 m below the tip of the leader ($z_0 = 250$ m), which corresponds to the real ground; and three intermediate cases: (iii) $z_0 = 650$ m, (iv) $z_0 = 1250$ m and (v) $z_0 = 3250$ m. In all cases considered in Section 3.3.2, the effects of the wind turbine receptors and down conductors are ignored to facilitate comparisons with the analytical model (13). The total charge on the leader is determined by integrating (8) along the leader, where $I_{peak} = 200$ kA corresponds to the lightning protection level LPL I. The FEA results for the case where the ground is set at infinity ($z_0 = \infty$) are compared to the analytical model (13) and are used primarily for verification purposes.

Figure 8 shows the calculated magnitude of the electric field along the blade *OA* for five different cases. As one can see, a good agreement exists between the analytical model and FEA results for the case when ground is set at infinity, $z_0 = \infty$. It is also shown that in the case of the real ground, $z_0 = 250$ m, the magnitude of the electric field is considerably higher than in the case when $z_0 = \infty$. Although applicability of the results presented in Figure 8 is limited due to the imposed assumptions regarding charge density and effects of the receptors and down conductors, these results provide some qualitative insight into the effect of the distance between the tip of the leader and the ground. The next section considers a more realistic case, where (i) wind turbine receptors and down conductors are taken into account by applying ground potential at the wind turbine and (ii) non-uniform charge density distribution along the leader is considered.

3.3.3. FEA results for the case of the non-uniform charge density.

A lightning stepped leader with a non-uniform charge density distribution (8) is considered, and FEA is performed to calculate electric fields along the wind turbine blades *OA*, *OB* and *OC*, as shown in Figure 7. An analysis of the problem

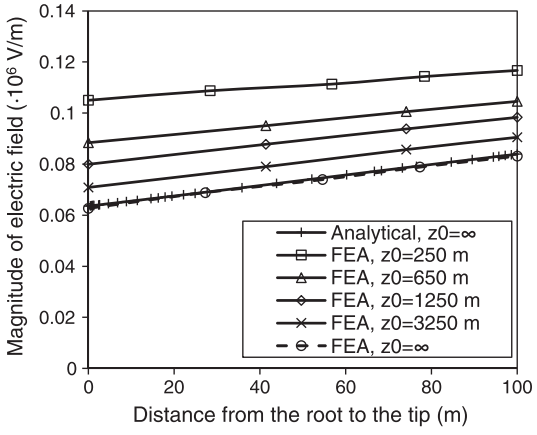

Figure 8. The magnitude of the electric field along blade *OA* due to a leader with a uniform charge density, LPL I (I_{peak} = 200 kA): effect of the distance between the tip of the leader and the ground.

formulated in Section 3.1 is performed. In this case (unlike the cases described in Section 3.3.2), the effects of the wind turbine receptors and down conductors are taken into account by applying ground potential at the wind turbine exterior surface (i.e. tower and blade surfaces). The cloud voltage is taken as $V = 40$ MV.[16]

Figure 9 shows the magnitudes of the electric fields along blades *OA*, *OB* and *OC* at LPL I. It can be seen that the electric field at blade *OA* is generally larger than that at blades *OB* and *OC*. Figure 10 shows the magnitudes of the electric fields at blade *OA* for three LPL levels. Close examination of the electric fields at LPL I and LPL II reveals that along blade *OA*, the electric field at LPL I is higher than the electric field at LPL II except for the small region near the tip of blade *OA*. This can be further seen in Table III, where the magnitudes of the electric fields at the tips of the blades are shown. In spite of the higher peak current corresponding to LPL I, at the tip of blade *OA*, the magnitude of the electric field corresponding to LPL I is considerably lower than the magnitude of the electric field corresponding to LPL II. Some insight into this somewhat counterintuitive result can be given by checking equation (2) for the lightning strike distance. As it can be seen, the higher peak current is associated with the larger lightning strike distance. At the same time, the electric field strength decays with an increase in the lightning strike distance (see, e.g. (13)). Therefore, an increase in the lightning strike distance counterbalances an increase in the peak current. Last, Figure 11 shows a contour plot of the electric field magnitude distribution in the vicinity of the wind turbine at LPL III.

It is obvious that wind turbine geometry will affect predictions of the electric field. To illustrate this, the FEA was performed for a wind turbine with the blades represented by tapered beams. Figure 12 shows comparisons between electric fields for the blades represented by beams of constant cross section and for the blades represented by tapered beams of variable cross section. Electric fields are calculated along blade *OA* at LPL I. As one can see, the electric fields are similar for the distances up to 60 m from the root of the blade. For distances exceeding 60 m, the electric field along the tapered blade is larger. In particular, at the blade tip, the electric field in the case of the tapered blades is about 18% larger than

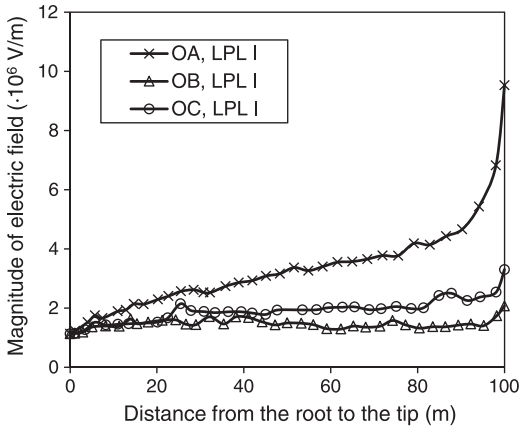

Figure 9. The magnitude of the electric field at blades *OA, OB, OC*, LPL I.

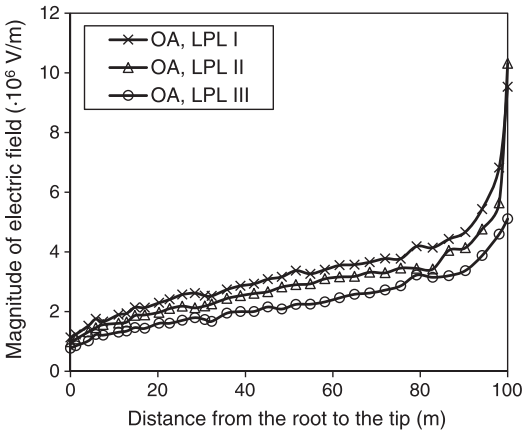

Figure 10. The magnitude of the electric field along blade *OA* for different LPL levels.

Table III. The magnitude of the electric field at the wind turbine blade tips and at the tip of the non-uniformly charge lightning stepped leader (z_0 = 250 m).

LPL	Peak current, I_{peak} (kA)	Magnitude of the electric field (V/m)			
		Blade *OA* tip	Blade *OB* tip	Blade *OC* tip	Lightning stepped leader tip
I	200	$9.53 \cdot 10^6$	$2.07 \cdot 10^6$	$3.30 \cdot 10^6$	$1.99 \cdot 10^7$
II	150	$1.03 \cdot 10^7$	$1.58 \cdot 10^6$	$2.81 \cdot 10^6$	$1.52 \cdot 10^7$
III	100	$5.10 \cdot 10^6$	$1.30 \cdot 10^6$	$1.66 \cdot 10^6$	$1.04 \cdot 10^7$

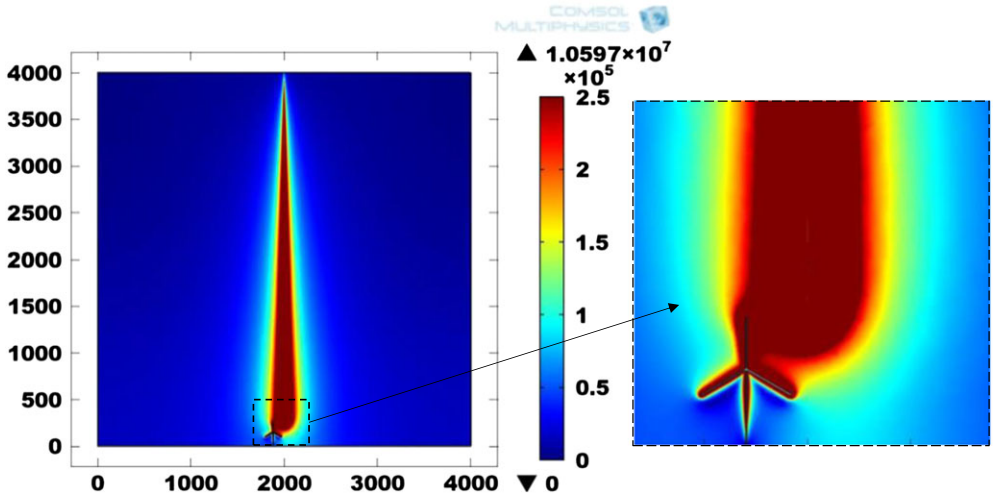

Figure 11. Electric field magnitude distribution in the vicinity of the wind turbine at LPL III. [Colour figure can be viewed at wileyonlinelibrary.com]

in the case of the constant cross-section blades. The largest discrepancy between fields (amounting to 25%) occurs at 88 m from the root.

3.4. Dielectric breakdown assessment in a non-conductive composite blade

Madsen[18] conducted an extensive experimental study to determine the dielectric breakdown strength of the glass fiber reinforced polymer matrix composite laminates used in the wind turbine blades. Based on the analysis of the experimental

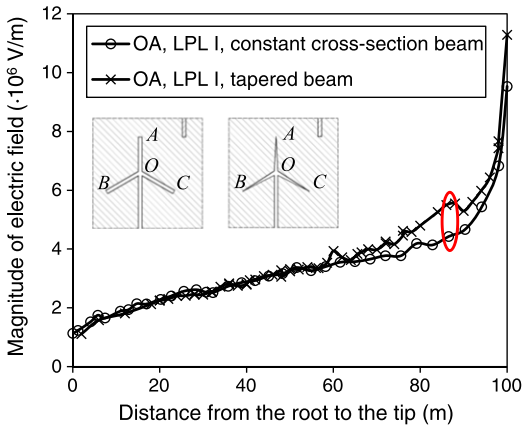

Figure 12. Effect of the geometry on the electric fields along blade *OA*, LPL I: tapered beam vs. constant cross-section beam. [Colour figure can be viewed at wileyonlinelibrary.com]

data, he suggested the empirical relationship between the dielectric breakdown strength and the thickness of the glass fiber polymer matrix composite laminate:

$$E_b = c_1 \cdot \frac{1}{t} + C_2 \cdot TI, \tag{14}$$

where E_b is the average breakdown field strength of the composite laminate (in V/m), t is the thickness of the laminate (in m), c_1 and C_2 are constants and TI is the tracking index, which depends on the fiber and matrix properties, fiber orientation, surface defects and wide erosion. In addition, the values of tracking index can vary from blade to blade due to uncertainties related to manufacturing and handling.[25] In this work, we assumed that the tracking index is a constant and the following parameters for the remaining constants were used: $c_1 = 5.3 \cdot 10^4$ and $c_2 = C_2 \cdot TI = 8.0 \cdot 10^6$. These parameter values were chosen based on the analysis of the experimental data on glass fiber polymer matrix composite laminate specimens.[18] Figure 13 shows comparisons between experimental data[18] for the specimens ranging in thickness from 2 mm to 6 mm[18] and predictions obtained using equation (14) with $c_1 = 5.3 \cdot 10^4$ and $c_2 = 8.0 \cdot 10.^6$ As one can see, a good agreement exists.

As for using equation (14) for calculating dielectric breakdown strength in wind turbine blades, caution should be exercised as thickness of the most sections of the blade exceeds 6 mm. In the present study, dielectric breakdown strength of the Sandia 100 m All-glass Baseline Wind Turbine Blade (SNL 100-00)[23] is evaluated. Planform of the blade is shown in Figure 14. The root buildup and spar cap of the blade are made of glass fiber reinforced polymer matrix composites. The other parts of the blade are made of sandwich panels with foam core and glass fiber polymer matrix composite facesheets. The experimental data on the dielectric breakdown strength of the sandwich composites is not available, so only the root buildup and spar cap sections are included in the analysis. Moreover, the blade is divided into 34 sections along the spanwise direction. Thicknesses of the root buildup and spar cap at various sections along the spanwise direction are shown in Table IV and Figure 15. As one can see, within 6 m from the blade tip, the thickness of the spar cap is less than 6 mm.

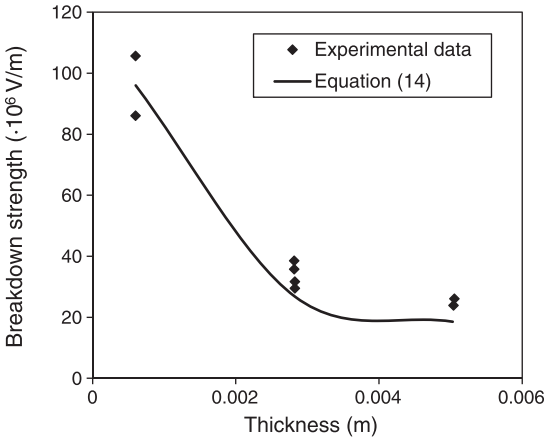

Figure 13. Dielectric breakdown strength of the glass fiber reinforced composite laminate.

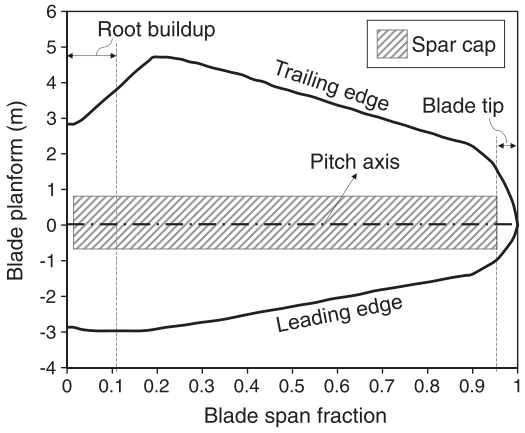

Figure 14. Sandia 100 m All-glass Baseline Wind Turbine Blade (SNL 100-00) planform.[23]

Table IV. Composite laminate thickness at various sections of the wind turbine blade.[23]

Section number	Blade span	Overall thickness (mm)	
		Root buildup	Spar cap
1	0.000	170	
2	0.005	150	1
3	0.007	130	2
4	0.009	110	3
5	0.011	90	4
6	0.013	80	10
7	0.024	73	13
8	0.026	65	13
9	0.047	50	20
10	0.068	35	30
11	0.089	25	51
12	0.114	15	68
13	0.146		94
14	0.163		111
15	0.179		119
16	0.195		136
17	0.222		136
18	0.249		136
19	0.277		128
20	0.358		119
21	0.439		111
22	0.521		102
23	0.602		85
24	0.667		68
25	0.683		64
26	0.732		47
27	0.765		34
28	0.846		17
29	0.895		9
30	0.944		5
31	0.957		5
32	0.972		5
33	0.986		5
34	1.000		

Therefore, equation (14) can be applied in this region to predict dielectric breakdown strength. At the same time, according to the results presented in Figures 9, 10 and 12, the region adjacent to the tip is also the most critical region, as the blade tip experiences the largest electric field.

Dielectric breakdown strengths of the spar cap in the vicinity of the blade tip were calculated using equation (14) and compared to the magnitudes of the electric fields along the tapered blade *OA* obtained using FEA. The corresponding safety factors at LPL I, i.e. ratios of the dielectric breakdown strength to the magnitude of the electric field, are shown in Figure 16 . As one can see, the safety factor at the tip of blade *OA* is 1.32 at the most severe LPL I.

It can be shown that tip of blade *OA* has the highest risk of experiencing dielectric breakdown. Let us assume that the safety factor calculated at the tip of blade *OA* is applied to other parts of the blade. Knowing electric field distribution along the entire blade (see Figure 12, the case of tapered beam), the presumed dielectric breakdown strength corresponding to the safety factor equal to 1.32 can be calculated. This results in values of the dielectric breakdown strength in the range from $0.85 \cdot 10^6$ V/m (at the root) to $7.19 \cdot 10^6$ V/m (at 10.5 m from the tip of the blade) that are unrealistically low. This, in turn, means that in reality the safety factors in the regions further from the blade tip are larger and, indeed, the tip of blade *OA* has the highest risk of experiencing dielectric breakdown. Recall that electric fields along blades *OB* and *OC* are weaker than along blade *OA*. Overall, blade *OA* is the most vulnerable to dielectric breakdown.

It is worth mentioning that the dielectric breakdown strength of composites may deteriorate during the service lifetime of the wind turbine blades due to the presence of moisture, defect accumulation, etc. Although experimental data specific to the composite wind turbine blades are not available, laboratory studies of the glass reinforced composites may be useful to assess the extent of deterioration in properties. For instance, experimental results reported in[26] indicate that Cyanate

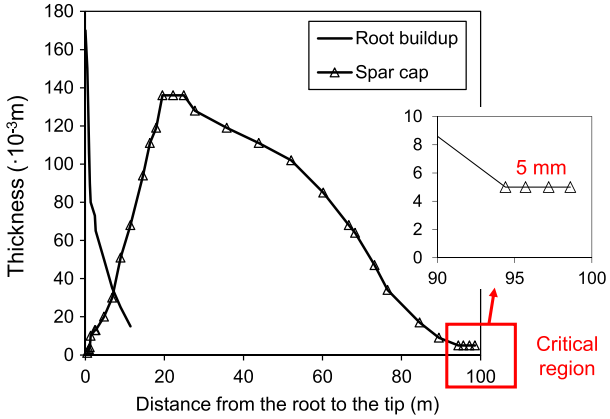

Figure 15. Composite laminate thickness distribution along the wind turbine blade. [Colour figure can be viewed at wileyonlinelibrary.com]

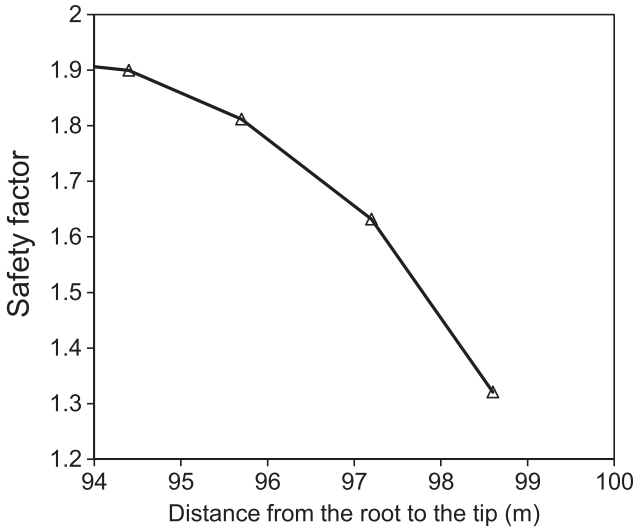

Figure 16. Safety factor (ratio between estimated dielectric breakdown strength and electric field) at LPL I for wind turbine blade *OA* spar cap in the vicinity of the blade tip.

Ester/S2 glass composite retains 90% of its dielectric strength after six-month exposure to 99% humidity. Hong *et al.*[27] observed a significant reduction in the breakdown strength in the specimens with 1.5% water content (the specimens were immersed in water until their weight increased by 1.5%). The dielectric strength measured in the specimens containing 1.5% of water was 20 kV/mm compared to 60 kV/mm for the dry specimens. Figure 16 shows that if the breakdown strength is reduced three times, the safety factor at the tip region of the spar cap of blade *OA* (90–100 m from the blade root) falls below one at LPL I and at LPL II. Therefore, dielectric breakdown and severe structural damage are likely to occur. Although investigation of the deterioration effects on the dielectric breakdown strength is beyond the scope of this study, the results obtained in this work suggest that the tip region of Sandia 100 m All-glass Baseline Wind Turbine Blade (SNL 100-00) is the most vulnerable to dielectric breakdown.

It should be mentioned that if dielectric breakdown does not occur in the composite laminated blades, lightning attachments will come as a direct heat injection into the surface of the non-conductive blades. The direct heat injection can produce a considerable damage that is manifested by thermal ablation, internal explosion, delamination, etc. For instance, experimental studies[28–30] suggest that an internal explosion occurs from interlaminar pressure buildup owing to the formation of pyrolysis gases. The pyrolysis gases are formed in the process of the interlaminar resin decomposition caused by the direct heat injection.

As a part of damage prediction due to lightning-induced heat injection, a heat transfer problem needs to be solved.[31] A heat transfer problem formulation for non-conductive structures (prior to the dielectric breakdown) is different from the one

for conductive structures (once the dielectric breakdown occurred). In the conductive structures, a heat transfer equation has to be solved simultaneously with electrodynamics equations to determine the distribution of the electric current and associated Joule heat densities. The direct heat injection into a structure from the lightning channel will still be a part of the heat transfer problem in the case of the conductive structure. In any case, careful analysis of the lightning-induced electric fields is essential for formulation of the physics-based thermo-mechanical damage models and is critical for development of damage tolerant composite blade designs.

4. CONCLUSION

In this paper, the electric fields in the wind turbine blades due to lightning stepped leader were analyzed at the different lightning protection levels and the dielectric breakdown was assessed. A horizontal axis wind turbine with three blades representing Sandia 100 m All-glass Baseline Wind Turbine Blades (SNL 100-00) was considered. The FEA analysis included the full length of the leader and enabled us to incorporate various uniform and non-uniform charge density models. The FEA results were verified by comparing the calculated electric fields with those predicted by the analytical model for the case of the uniform charge density. The dielectric breakdown strength of the blades was evaluated based on the experimental data. Ratios (safety factors) of the dielectric breakdown strength to the electric field were calculated along all three blades and were used to assess the conservativeness of the blade design against the dielectric breakdown. The results show that the tip region of the blade is the most vulnerable to the dielectric breakdown with the safety factor as low as 1.32 at LPL I. Possible deterioration in the dielectric breakdown strength of composites during the service lifetime of the wind turbine blades due to the presence of moisture, defect accumulation, etc., will lead to even lower safety factors.

ACKNOWLEDGEMENT

We would like to acknowledge the support from the National Science Foundation under Grant Number EPS-1101284. Any opinions, findings, conclusions or recommendations expressed in this work are those of the author and do not necessarily reflect the views of the National Science Foundation.

REFERENCES

1. Rupke E. Lightning direct effects handbook. *Lightning Technologies Inc. Report No. AGATE-WP3*, 2002: 1-031027.
2. GCube top 5 US wind energy insurance claims report. Available from: http://www.gcube-insurance.com/en/press/gcube-top-5-us-wind-energy-insurance-claims-report/ (Accessed by November 2015).
3. Cotton I, Jenkins N, Pandiaraj K. Lightning protection for wind turbine blades and bearings. *Wind Energy* 2001; **4**(1): 23–37.
4. Xiaohui W, Zhang X. Calculation of electromagnetic induction inside a wind turbine tower struck by lightning. *Wind Energy* 2010; **13**(7): 615–625.
5. Veers PS, Ashwill TD, Sutherland HJ, Laird DL, Lobitz DW, Griffin DA et al. Trends in the design, manufacture and evaluation of wind turbine blades. *Wind Energy* 2003; **6**(3): 245–259.
6. Rakov VA, Uman MA. *Lightning: Physics and Effects*. Cambridge University Press: New York, 2007.
7. Rakov VA. The physics of lightning. *Surveys in Geophysics* 2013; **34**(6): 701–729.
8. Larigaldie S, Labaune G, Moreau JP. Lightning leader laboratory simulation by means of rectilinear surface discharges. *Journal of Applied Physics* 1981; **52**(12): 7114–7120.
9. Larigaldie S. Spark propagation mechanisms in ambient air at the surface of a charged dielectric. I. Experimental: The main stages of the discharge. *Journal of Applied Physics* 1987; **61**(1): 90–101.
10. Larigaldie S, Roussaud A, Jecko B. Mechanisms of high-current pulses in lightning and long-spark stepped leaders. *Journal of Applied Physics* 1992; **72**(5): 1729–1739.
11. Golde RH. The frequency of occurrence and the distribution of lightning flashes to transmission lines. *Electrical Engineering* 1945; **64**(12): 902–910.
12. Golde RH. *Lightning Protection*. Edward Arnold: London, UK, 1973.
13. Cooray V, Rakov V, Theethayi N. The lightning striking distance—revisited. *Journal of Electrostatics* 2007; **65**(5): 296–306.
14. Uman MA. *The Lightning Discharge* (second edn). Dover Publications Inc.: New York, 2001.

15. Zhou H, Diendorfer G, Thottappillil R, Pichler H, Mair M. Characteristics of upward positive lightning flashes initiated from the Gaisberg Tower. *Journal of Geophysical Research. Atmospheres* 2012; **117**: D6.
16. Becerra M. On the attachment of lightning flashes to grounded structures. *PhD Thesis*, Uppsala University, 2008.
17. Lewke B, Hernández YM, Kindersberger J. A simulation method for the wind turbine's electric field distribution caused by the stepped lightning leader. *European Wind Energy Conference & Exhibition* (*EWEC*), Milan, Italy, 7–10 May 2007.
18. Madsen S. Interaction between electrical discharges and materials for wind turbine blades—particularly related to lightning protection. *PhD Thesis*, The Technical University of Denmark, 2006.
19. IEC 61400-24 ed1.0, Wind turbine generator systems—part 24: lightning protection; IEC/TR 61400-24:2002(E).
20. Eriksson AJ. The lightning ground flash—an engineering study. *PhD thesis*, University of Natal, Pretoria (CSIR Special Report ELEK 189), 1979.
21. Eriksson AJ. The incidence of lightning strikes to power lines. *Power Delivery, IEEE Transactions on* 1987; **2**(3): 859–870.
22. D'Alessandro F, Petrov NI. Field study on the interception efficiency of lightning protection systems and comparison with models. *In Proceedings of the Royal Society of London A*: *Mathematical*, *Physical and Engineering Sciences* 2006; **462**(2069): 1365-1386. The Royal Society.
23. Griffith DT, Ashwill TD. The Sandia 100-meter all-glass baseline wind turbine blade: SNL100-00. *Sandia National Laboratories*: *SANDIA REPORT*, SAND2011-3779, 2011.
24. Tipler PA, Mosca G. *Physics for Scientists and Engineers*. Macmillan: New York, 2007.
25. Madsen SF, Holboell J, Henriksen M, Bjaert N. Tracking tests of Glass Fibre Reinforced Polymers (GRP) as part of improved lightning protection of wind turbine blades. *In 27th International Conference on Lightning Protection*, Avignon, France, 13–16 September 2004.
26. Morgan B, Madhukar M, Walsh J, Hooker M, Grandlienard S. Moisture degradation of cyanate ester/S2 glass composite insulation systems. *Journal of Composite Materials* 2010; **44**(7): 821–837.
27. Hong TP, Lesaint O, Gonon P. Water absorption in a glass–mica–epoxy composite I: influence on electrical properties. *IEEE Transactions on Dielectrics and Electrical Insulation* 2009; **16**(1): 1–10.
28. Feraboli P, Miller M. Damage resistance and tolerance of carbon/epoxy composite coupons subjected to simulated lightning strike. *Composites Part A: Applied Science and Manufacturing* 2009; **40**(6): 954–967.
29. Hirano Y, Katsumata S, Iwahori Y, Todoroki A. Artificial lightning testing on graphite/epoxy composite laminate. *Composites Part A: Applied Science and Manufacturing* 2010; **41**(10): 1461–1470.
30. Li Y, Li R, Lu L, Huang X. Experimental study of damage characteristics of carbon woven fabric/epoxy laminates subjected to lightning strike. *Composites Part A: Applied Science and Manufacturing* 2015; **79**: 164–175.
31. Wang Y, Zhupanska OI. Lightning strike thermal damage model for glass fiber reinforced polymer matrix composites and its application to wind turbine blades. *Composite Structures* 2015; **132**: 1182–1191.